JOURNAL OF MATERIALS SCIENCE 16 (1981) 3427–3436

A re-investigation of the thermal decomposition of ammonium paratungstate

G. J. FRENCH, F. R. SALE
Metallurgy Department, University of Manchester, Manchester, UK

The thermal decomposition of monoclinic ammonium paratungstate (APT) and amorphous ammonium metatungstate (AMT) has been studied over the temperature range 20 to 500° C using thermogravimetry, evolved gas analysis, X-ray diffraction analysis, differential thermal analysis and scanning electron microscopy. A mechanism of decomposition which postulates the formation and subsequent decomposition of various lower ratio tungstates is proposed and substantiated by the experimental data.

1. Introduction

The production of tungsten metal powder or tungsten carbide for the cutting tool industry relies upon the reduction of tungsten trioxide. Traditionally the tungsten trioxide may be obtained by the thermal decomposition of either tungstic acid or, for higher purity applications, by the thermal decomposition of ammonium paratungstate (APT). A simplified flow sheet for the production of tungstic acid and ammonium paratungstate from ore concentrates is shown in Fig. 1. The structure and morphology of the APT crystals obtained as a result of the process outlined in Fig. 1 depend upon the temperature and type of crystallization technique used in the final stages of the process. The structures and morphologies of various commercial forms of APT have been reported previously [1], where it was shown that both high-temperature crystallization and evaporation produce the monoclinic pentahydrate form of APT, $5(NH_4)_2O \cdot 12WO_3 \cdot 5H_2O$, which has a "cuboid" equi-axed monoclinic powder morphology, whereas room-temperature crystallization produces the orthorhombic undecahydrate, $5(NH_4)_2 \cdot 12WO_3 \cdot 11H_2O$, form of APT, which has a lath-like morphology. Freeze-dried APT was shown to have an amorphous multiparticulate structure with a chemical composition similar to the undecahydrate.

The particle size and morphology of the APT is of some importance because the WO_3 produced by thermal decomposition is obtained as a pseudomorph of the original APT, the size of which may ultimately affect the kinetics of the reduction process. Also it is possible to carry this pseudomorph over into the metal product which is obtained at the end of the reduction process [2–5]. Consequently, a preliminary study was made a number of years ago of the morphological aspects of the thermal decomposition of ammonium paratungstate in its various forms [6]. During the course of this earlier study thermogravimetric measurements, using a glass spring thermobalance, and isothermal mass spectrometric evolved gas analysis measurements were also made of the thermal decomposition and a mechanism of decomposition was postulated which involved the production of ammonium metatungstate. The present paper reports both a re-investigation of the thermal decomposition process of ammonium paratungstate, using more sophisticated thermal analytical equipment, and a study of the decomposition of ammonium metatungstate, in order to explain a number of previously unexplained observations concerning the decomposition of these industrially important materials.

2. Experimental procedure

2.1. Materials

Both the ammonium paratungstate (APT) and the ammonium metatungstate (AMT) were of normal accepted purity for pure tungsten metal manufacture (as reported previously [1]) and were supplied by Murex Ltd, Rainham, Essex. X-ray diffraction analysis showed the APT to be the monoclinic pentahydrate form, $5(NH_4)_2O \cdot 12WO_3 \cdot 5H_2O$,

0022–2461/81/123427–10$03.00/0

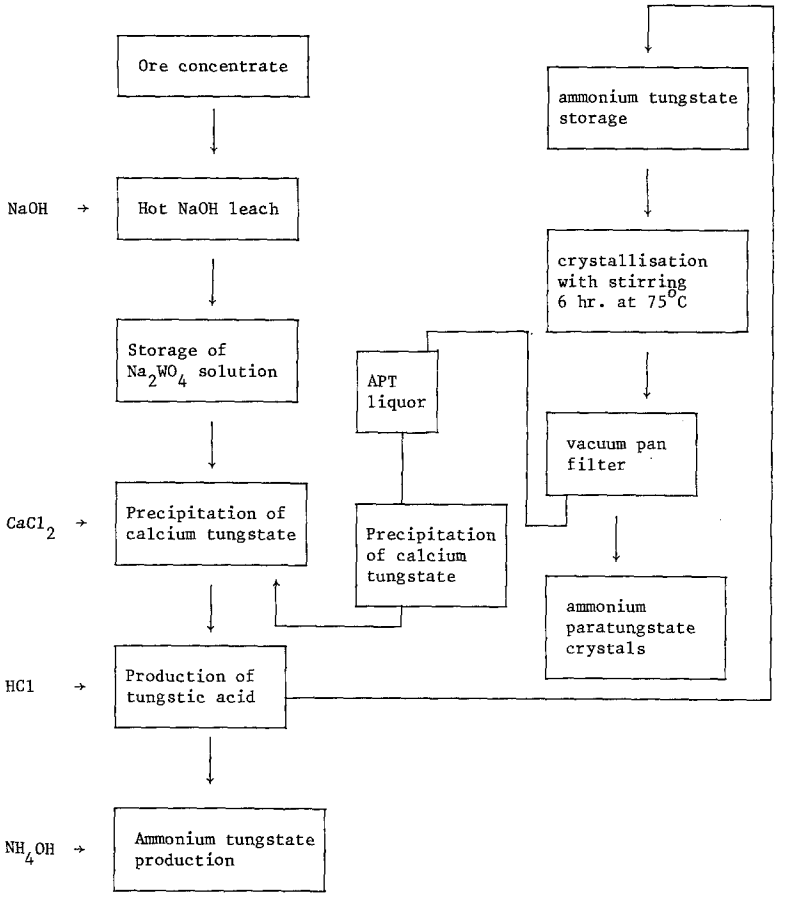

Figure 1 Simplified flow diagram showing the production of ammonium paratungstate.

whilst the AMT was shown to be amorphous. The AMT was supplied with the quoted formula of $3(NH_4)_2O \cdot 12WO_3 \cdot 10H_2O$, which was shown to be correct by thermogravimetric analysis (see the following section). Both samples were studied in a Cambridge Instruments-S4 scanning electron microscope in order to determine their particle sizes and morphologies. Figs 2 and 3 show representative scanning electron micrographs of the APT and AMT, respectively.

2.2. Thermogravimetric analysis (TGA)

A Cahn R.H. thermogravimetric electrobalance was used in conjuction with a Nichrome wound furnace which was controlled by a Newtronic Electronics scanning temperature controller. The furnace was also able to be traversed in the vertical direction thus allowing the decomposition of a sample to be arrested at any desired temperature and also allowing the easy retrieval of partially and fully decomposed samples for characterization by X-ray diffraction analysis and scanning electron microscopy.

The thermal decompositions of both the APT and AMT were carried out under an atmosphere of "white spot" nitrogen. The apparatus was first evacuated to a pressure of < 0.5 mbar after which

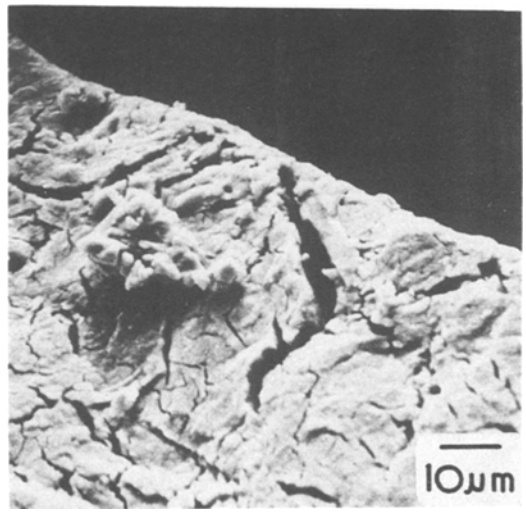

Figure 2 Scanning electron micrograph of the equi-axed monoclinic APT.

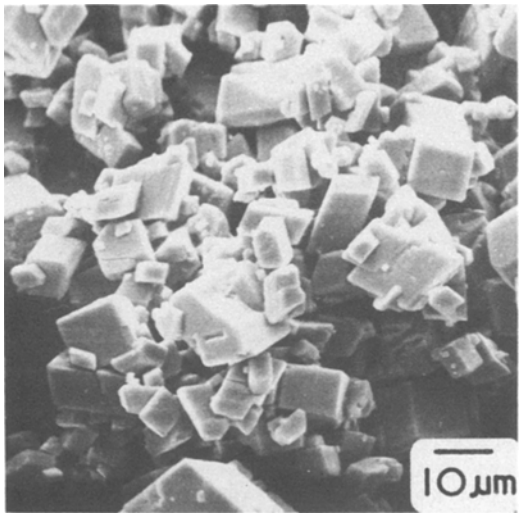

Figure 3 Scanning electron micrograph of the AMT.

it was back-filled to atmospheric pressure and thereafter the nitrogen flow was kept at 200 $cm^3 min^{-1}$. Sample weights of 290 mg were heated at a rate of 5° C min^{-1} up to a maximum temperature of 500° C. The sensitivity of the thermobalance was of the order of 0.1 mg using a 40 mg full-scale deflection. These settings allowed weight losses of up to 14% to be observed on a single scale of the balance. After decomposition the furnace was lowered and the samples were allowed to cool in the nitrogen atmosphere.

2.3. Evolved gas analysis (EGA)

Evolved gas analysis was carried out using a VG Micromass 6 mass spectrometer in conjunction with a furnace that was controlled by a Stanton-Redcroft linear temperature programmer. The mass spectrometer was set to scan magnetically between *m/e* values of 16 and 18 at a frequency of one scan every 30 sec. The accelerating voltage was fixed at 1.5 kV. The detection system was a Faraday cage used in conjunction with a chopper amplifier. The response time of the system was 1 sec and the resolution was approximately 400 at mass 40.

In operation, approximately 100 mg of sample was placed in the bottom of a 6 mm diameter silica tube which was attached to the analyser head of the mass spectrometer by a 0.5 m length of 0.8 mm diameter stainless steel capillary tubing. The specimen tube was continuously pumped via the capillary tube and gas samples were taken through a calibrated leak into the analyser head. The temperature of the sample was increased at a rate of 200° C h^{-1} up to a maximum of 600° C.

2.4. X-ray diffraction analysis

X-ray diffraction analysis of the as-received samples and the products of partial and full decomposition were carried out on a Phillips horizontal diffractometer scanning over the range 15° to 90° at a rate of 1° min^{-1} using CuKα radiation.

2.5. Differential thermal analysis (DTA)

The decompositions of both APT and AMT were studied in a Stanton-Redcroft DTA unit, model 673-4. Sample weights of 50 mg, sandwiched between 25 g layers of alumina powder, were heated in Inconel crucibles from room temperature to 600° C at a rate of 5° C min^{-1} in a nitrogen atmosphere. Calcined, powdered alumina (100 mg) was used as the reference material.

2.6. Particle morphology

In addition to the characterization of the as-received samples, (as outlined in a previous section), the characterization of the particle morphologies of partially decomposed and fully decomposed products was carried out using a Cambridge S4 scanning electron microscope to determine whether significant changes occurred during the decomposition process. The samples were prepared by sprinkling on to aluminium paint on the specimen stub of the microscope. To ensure that charging of the specimens did not occur in the microscope they were sputter-coated with gold.

3. Results

3.1. Thermogravimetric determinations

The results of the thermogravimetric determinations of the decomposition process, expressed as the relationship between percentage weight loss and temperature, are shown in Figs 4 and 5 for APT and AMT, respectively. From Fig. 4 it can be seen that the thermal decomposition of the APT occurs in four separate stages:

Stage 1 – occurs between room temperature and 100° C with a corresponding weight loss of 2.29%.

Stage 2 – occurs between 180 and 225° C with a corresponding weight loss of 2.16%.

Stage 3 – occurs between 230 and 325° C with a corresponding weight loss of 5.04%.

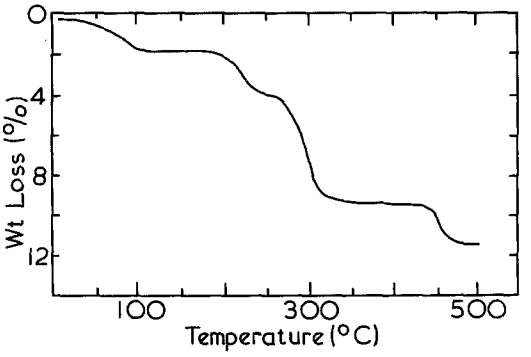

Figure 4 TG curve for APT.

Stage 4 – occurs between 440 and 500° C with a corresponding weight loss of 1.65%.

After Stage 4 the decomposition is complete and no further weight losses occur. The end of each stage is characterized by a clearly defined plateau region over which the material is thermally stable. The total experimental weight loss of 11.14% is in good agreement with the theoretically predicted value of 11.11%.

Fig. 5 shows that the thermal decomposition of the AMT sample occurs in three clearly defined stages:

Stage 1 – occurs between room temperature and 150° C with a corresponding weight loss of 4.03%, (a minor inflection in the weight-loss curve may be seen at approximately 110° C).

Stage 2 – occurs between 225 and 375° C with a corresponding weight loss of 5.06%.

Stage 3 – occurs between 440 and 500° C with a corresponding weight loss of 1.66%.

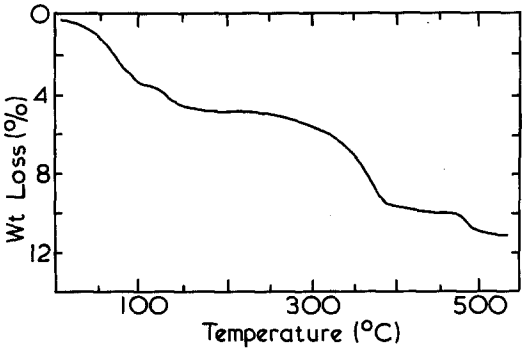

Figure 5 TG curve for AMT.

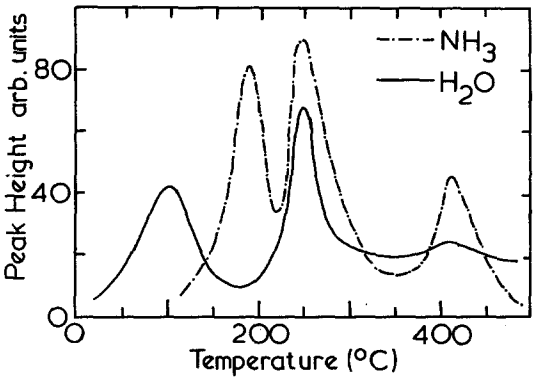

Figure 6 EGA curve for APT.

The experimentally determined weight loss for the production of WO_3 was 10.75% which agrees well with the theoretically predicted value of 10.70% based on the stoichiometry of the AMT.

It is evident from Figs 4 and 5 that at temperatures above 225° C the shapes of the thermogravimetric curves for both APT and AMT are very similar which indicates that the latter stages of decomposition of each compound may be identical.

3.2. Evolved gas analysis

The output from the mass spectrometer was corrected for background and for the cracking patterns of H_2O and NH_3 to give the data that is presented in Figs 6 and 7, respectively, for APT and AMT. As with the results of thermogravimetric studies it can be seen that APT decomposes in four separate stages. The temperatures determined in the EGA are in quite good agreement with those determined using the thermobalance. It is apparent from the separate traces for H_2O and NH_3 shown in Fig. 6, that at temperatures up to 100° C there is a rapid evolution of H_2O which decreases rapidly as the temperature is increased

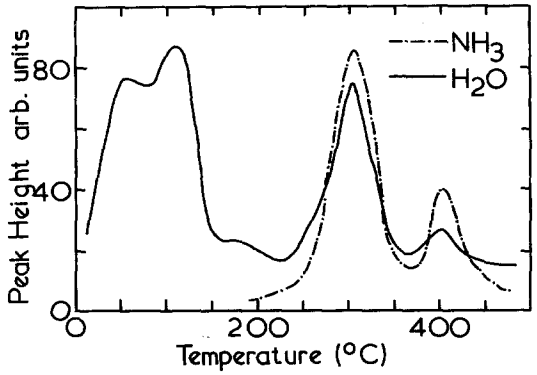

Figure 7 EGA curve for AMT.

TABLE I *d*-spacings and intensities of major lines obtained on decomposition of APT

As received			Decomposition temperature								
			125° C			225° C	350° C	450° C			
d-spacing	I/I_1	Phase	*d*-spacing	I/I_1	Phase			*d*-spacing	I/I_1	Phase
10.12	100	Monoclinic APT	5.08	100	Monoclinic APT	No diffraction pattern	No diffraction pattern	3.82	90	WO_3
5.10	100	Monoclinic APT	4.79	42	Monoclinic APT			3.74	90	$WO_{2.9}$
4.80	45	Monoclinic APT	4.41	3	Monoclinic APT			3.63	100	WO_3
4.30	15	Monoclinic APT	4.31	16	Monoclinic APT			3.32	22	WO_3
4.16	25	Monoclinic APT	4.15	20	Monoclinic APT			3.07	37	WO_3
3.60	20	Monoclinic APT	3.91	12	Monoclinic APT			2.66	60	$WO_{2.9}$
3.40	20	Monoclinic APT	3.60	37	Monoclinic APT			2.61	75	WO_3
3.36	25	Monoclinic APT	3.54	40	Monoclinic APT			2.50	12	WO_3
3.15	70	Monoclinic APT	3.49	36	Orthorhombic APT			2.15	25	WO_3
3.02	30	Monoclinic APT	3.42	26	Monoclinic APT			2.01	10	WO_3
2.97	50	Monoclinic APT	3.36	30	Monoclinic APT			1.98	7	WO_3
2.89	50	Monoclinic APT	3.17	85	Monoclinic APT			1.91	12	WO_3
2.71	20	Monoclinic APT	2.97	57	Monoclinic APT			1.87	12	WO_3
2.64	20	Monoclinic APT	2.87	55	Monoclinic APT			1.82	32	WO_3
2.51	40	Monoclinic APT	2.73	25	Monoclinic APT			1.70	17	WO_3
–	–	–	2.62	20	Monoclinic APT			1.68	17	WO_3
–	–	–	2.51	33	Monoclinic APT			1.67	22	WO_3
–	–	–	2.46	46	Orthorhombic APT			1.64	35	WO_3

TABLE II *d*-spacings and intensities of major lines obtained on decomposition of AMT

As-received	Decomposition temperature					
	125° C	225° C	350° C	450° C		
				d-spacing	I/I_1	Phase
No diffraction pattern	No diffraction pattern	No diffraction pattern	No diffraction pattern	3.82	90	WO_3
				3.74	90	$WO_{2.9}$
				3.63	100	WO_3
				3.32	22	WO_3
				3.07	37	WO_3
				2.66	60	$WO_{2.9}$
				2.61	75	WO_3
				2.50	12	WO_3
				2.15	25	WO_3
				2.01	10	WO_3
				1.98	7	WO_3
				1.91	12	WO_3
				1.87	12	WO_3
				1.82	32	WO_3
				1.70	17	WO_3
				1.68	17	WO_3
				1.67	22	WO_3
				1.64	35	WO_3

to 200° C after which the H_2O evolution again increases to reach a peak value at 250° C. NH_3 begins to be evolved at 150° C, reaches a peak evolution at 190° C, after which the rate of evolution decreases rapidly and then rises again to give another peak at 250° C. At temperatures above 250° C the rates of evolution of both H_2O and NH_3 decrease and do not begin to increase again until approximately 380° C. The rates of evolution of both gases again reach maxima at temperature just above 400° C after which they both return to their background levels on reaching a temperature of 500° C.

The evolved gas analysis traces shown in Fig. 7 for AMT again support the equivalent thermogravimetric data. The initial stage of decomposition up to 150° C is associated solely with the evolution of H_2O. The partial separation of peaks in this initial stage was also evident in both the TG data and the DTA data and may possibly be caused by the formation and subsequent decomposition of metastable hydrated forms before complete dehydration is achieved. On heating further both H_2O and NH_3 begin to be evolved at temperatures of the order of 225° C and reach maximum rates of evolution at 300° C. The rates of evolution of both gases fall as the temperature is increased to 360° C after which further increases in rates of evolution occur with maxima at 400° C. As for the sample of APT, heating to temperatures above 400° C causes both gases to be reduced to their background levels at a temperature of approximately 500° C.

3.3. X-ray diffraction analysis

The results of the analyses of the various materials are presented in Tables I and II. The final decomposition products for both APT and AMT were yellow/blue in colour and as expected can be seen to be predominantly WO_3 with small traces of $W_{20}O_{58}$. Pure yellow WO_3 was obtained on decomposing both the APT and AMT in air, however, the small degree of reduction necessary to produce traces of $W_{20}O_{58}$ always occurred when the decomposition was carried out in nitrogen. It is apparent that the ammonia that is liberated during the final stages of decomposition cracks sufficiently to allow the small amount of reduction to occur. Decomposition of APT at 125° C can be seen to leave a crystalline product that yields a diffraction pattern composed mainly of lines that may be associated with monoclinic APT. Decomposition at 225 and 350° C yielded a material which was amorphous and did not produce any discernable diffraction pattern. Decomposition at 450° C yielded the final product of WO_3 plus traces of $W_{20}O_{58}$.

From Table II it is apparent that the AMT is amorphous in the as-received condition and only yields a discernable diffraction pattern after decomposition at temperatures in excess of

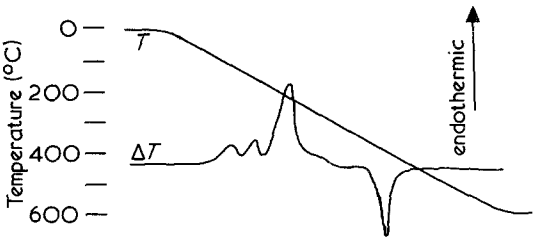

Figure 8 DTA curve for APT.

400° C. The lack of diffraction patterns for the intermediate products is in agreement with the observations reported for the APT.

3.4. Differential thermal analysis

As with the TG and EGA results, DTA showed separate decomposition steps for both APT and AMT and gave good agreement with the temperatures reported previously. Figs 8 and 9 show representative DTA traces for APT and AMT, respectively. From Fig. 8 it is apparent that the first three stages of decomposition of APT are all endothermic in nature, (which may be expected from typical gaseous evolution thermal decomposition reactions), however, the fourth stage of decomposition is strongly exothermic in nature and its appearance is not so easily explained. A similar exothermic peak is also evident in Fig. 9 for the AMT sample. The dehydration of the AMT sample can be seen to occur as a multi-stage process (as indicated in the evolved gas analysis) after which just one other clearly defined endothermic reaction occurs before the exothermic reaction.

4. Discussion

4.1. Mechanism of decomposition

4.1.1. APT

The experimental results, in combination, have shown that the overall mechanism of decomposition involves four separate stages, two of which are associated with the formation of amorphous intermediates before the final product of decomposition (WO_3) is obtained. During the first stage of decomposition, which occurs over the temperature range, room temperature to 100° C, a 2.29% weight loss has been determined (with a reproducibility of better than ± 0.05% over many different runs) and evolved gas analysis shows that only H_2O was evolved during this stage. It is apparent, therefore, that this is solely a dehydration stage, which stoichiometrically corresponds to the loss of 4 molecules of H_2O for every one molecule of monoclinic APT:

$$5(NH_4)_2O \cdot 12WO_3 5H_2O(c) \rightarrow 5(NH_4)_2O \cdot 12WO_3 \cdot H_2O(c) + 4H_2O(g). \quad (1)$$

X-ray diffraction analysis of the monohydrate indicates a crystalline solid of identical structure to the pentahydrate. Because only H_2O has been evolved the $(NH_4)_2O : WO_3$ ratio remains at 5 : 12 the accepted value for paratungstates.

The second stage of decomposition, which occurs over the temperature range 180 to 225° C and gives a weight loss of 2.16 wt %, is associated with the evolution of NH_3 only and the production of an amorphous solid phase. Stoichiometrically the weight loss is equivalent to the loss of 4 molecules of NH_3 for each molecule of the monohydrate:

$$5(NH_4)_2O \cdot 12WO_3 \cdot H_2O(c) \rightarrow 3(NH_4)_2O \cdot 12WO_3 \cdot 3H_2O(\text{amorphous}) + 4NH_3(g). \quad (2)$$

The amorphous solid product obtained as a result of this stage of the decomposition is ammonium metatungstate (AMT) (of the generally accepted $(NH_4)_2O : WO_3$ ratio of 1 : 4). The formation of AMT by the baking of crystalline APT in the temperature range 150 to 380° C has been reported previously [7, 8].

The third stage of decomposition, which occurs over the approximate temperature range 230 to 325° C and is associated with a 5.04% loss in weight, has been identified as being accompanied by the evolution of both NH_3 and H_2O. The most reasonable way in which the weight loss may be associated with the evolution of both gases and the stoichiometry of the AMT is to postulate that for every AMT molecule, four NH_3 molecules and five H_2O molecules are evolved. The theoretical percentage weight loss for this gaseous evolution is in excellent agreement with the experimentally determined value. The product of this stage of decomposition was determined to be amorphous

Figure 9 DTA curve for AMT.

and appears to be a previously unidentified anhydrous tungstate of $(NH_4)_2O:WO_3$ ratio of 1:12:

$$5(NH_4)_2O \cdot 12WO_3 \cdot 3H_2O(\text{amorphous}) \rightarrow (NH_4)_2O \cdot 12WO_3(\text{amorphous}) + 4NH_3(g) + 5H_2O(g). \quad (3)$$

Although an ammonium tungstate of this $(NH_4)_2O:WO_3$ ratio has not been identified previously, many variations of sodium metatungstate of ratios 1:8 and containing other large numbers, in the range 10 to 40, of WO_3 radicals have been discussed by Rieck [9]. Consequently, a variety of metatungstate of the general formula $M_2O:WO_3$ of 1:12 appears to be in keeping with these previous observations. In addition a crystalline, hexagonal ammonium tungsten bronze phase of stoichiometry $(NH_4)_{0.25}WO_3$ has been identified as a product of partial reduction of APT in dry hydrogen [10]. The form of the reduction curve given in this study [10] showed only one plateau at approximately 7 wt% loss and so was very different from that reported in the present study for decomposition in nitrogen. However, the hexagonal ammonium tungsten bronze has also been given by Dahl [11] as the reason for a high-temperature arrest (approximately 350 to 390° C) on thermogravimetric curves for the decomposition of APT in nitrogen, hydrogen, air and hydrogen/nitrogen atmospheres. This product was identified in the products of hydrogen reduction by X-ray diffraction analysis followed by comparison with the diffraction data presented previously [10]. The form of the thermogravimetric curve for the decomposition of APT in nitrogen shown by Dahl [11] is, however, almost identical to that determined in the present study and showed the various low-temperature plateaux evident in Fig. 7 as well as the high-temperature plateau (that was associated with the ammonium tungsten bronze) but was very different to that given for the production of the ammonium tungsten bronze [10]. In the present study the stable product at the 9.3% loss in weight was prepared on a number of separate occasions (from both APT and AMT) and each sample was studied using X-ray diffraction analysis. On no occasion was a diffraction pattern of any type obtained. Consequently, it appears that the ammonium tungsten bronze most probably occurs only as a product of decomposition/reduction of APT in hydrogen-containing atmospheres. Whereas, when the decomposition is carried out in nitrogen an amorphous tungstate of the ratio $(NH_4)_2O:WO_3$ of 1:12 is produced. Extra evidence for the amorphous nature of this phase may also be obtained from the DTA data, as discussed below. It is also interesting to note that the ammonium tungsten bronze was reported as a dark-coloured lustrous solid phase [10]. The amorphous compound found in the present study was off-white in colour and did not possess a metallic lustre.

The fourth and final stage of decomposition occurs over the temperature range 400 to 500° C and is accompanied by a weight loss of 1.65%. Evolved gas analysis shows that small amounts of both NH_3 and H_2O are liberated at this stage and the experimental weight loss may be attributed to the liberation of 2 molecules of NH_3 and one molecule of H_2O. Such evolution would leave WO_3 as the final product of decomposition:

$$(NH_4)_2O \cdot 12WO_3(\text{amorphous}) \rightarrow 12WO_3(c) + 2NH_3(g) + H_2O(g). \quad (4)$$

This postulated reaction step is consistent with the data obtained by DTA, as well as that obtained by the other techniques. It was outlined previously that the first three stages of decomposition were all significantly endothermic in nature whilst the final stage was exothermic (Fig. 8). It is apparent from the reaction proposed for the final stage of decomposition that an exothermic contribution analogous to an exothermic enthalpy of crystallization (amorphous solid → crystalline solid) must be included in the final stage in addition to the enthalpic requirement for gaseous evolution. Consequently, the overall heat effect for the final stage of decomposition is exothermic. Such effects have been reported by Berg [12] who has noted exothermic reactions for certain salts during decomposition when the reactions involved concern transformations of an amorphous anhydrous phase into a crystalline one.

4.1.2. AMT

It can be seen from the previous section that AMT occurs as one of the products of decomposition in the mechanism proposed for APT. Consequently, it may be expected that the thermal decomposition of AMT prepared by a separate precipitation technique should agree in general with the latter stages of the decomposition of APT. The major difference between the behaviour of the precipitated

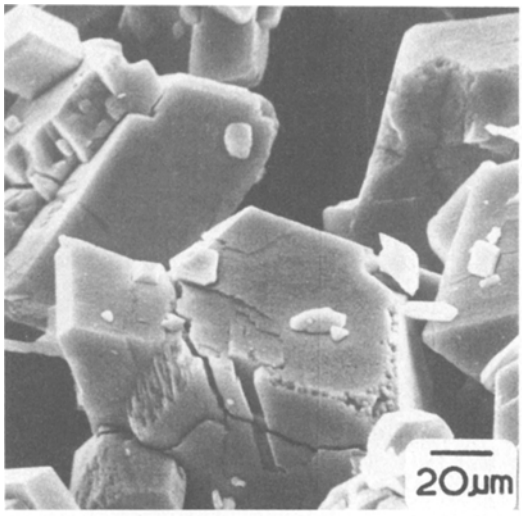

Figure 10 Scanning electron micrograph of the product of decomposition of APT at 500° C.

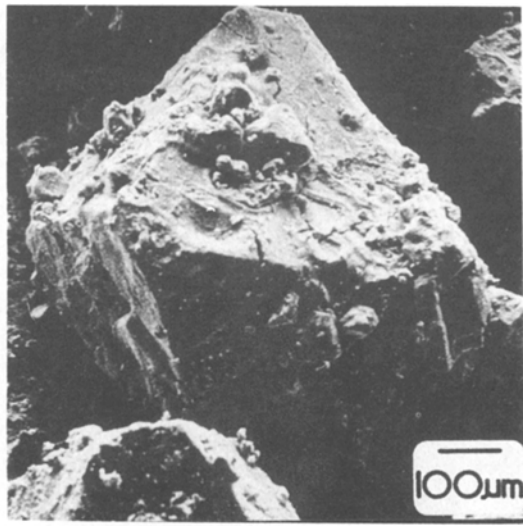

Figure 11 Scanning electron micrograph of the product of decomposition of AMT at 500° C.

AMT and that produced as the product of partial decomposition of APT may be attributed to dehydration of the precipitated sample at lower temperatures. Consequently, the decomposition of AMT may be summarized as:

(*a*) *Dehydration (room temperature to 150° C).*

$$3(NH_4)_2O \cdot 12WO_3 \cdot 10H_2O(\text{amorphous}) \rightarrow 3(NH_4)_2O \cdot 12WO_3 \cdot 3H_2O(\text{amorphous}) + 7H_2O(g) \ldots \text{Endothermic.} \quad (5)$$

(*b*) *Transformation to (1:12) ratio tungstate (225 to 375° C).*

$$3(NH_4)_2O \cdot 12WO_3 \cdot 3H_2O(\text{amorphous}) \rightarrow (NH_4)_2O \cdot 12WO_3(\text{amorphous}) + 4NH_3(g) + 5H_2O(g) \ldots \text{Endothermic.} \quad (6)$$

(*c*) *Final decompostion to yield WO_3 (440 to 500° C).*

$$(NH_4)_2O \cdot 12WO_3(\text{amorphous}) \rightarrow 12WO_3(c) + 2NH_3(g) + H_2O(g) \ldots \text{Exothermic.} \quad (7)$$

The stoichiometry of the latter two stages of this scheme are confirmed by the thermogravimetric and evolved gas analysis data and agree well with the behaviour of the AMT produced during thermal decomposition of the APT.

4.1.3. Particle morphology

The particle morphologies of the products obtained from APT in the present study agree substantially with those reported previously [1]. Monoclinic APT, having equi-axed uniform particles, yielded products of decomposition which in the majority of cases were simple cracked pseudomorphs of the original particles (Fig. 10). In a small number of cases the equi-axed crystals appear to have disintegrated into smaller irregular particles as stresses were built up in the crystals during the decomposition process, however, the overall morphology for the majority of the material is the same as the original APT. The important observations of the present study concern the amorphous AMT, which was initially in the form of irregular angular-shaped particles (Fig. 2). As for the APT, the major changes in particle morphology that occur during decomposition are associated with the formation of cracks (Fig. 11). However, the amount of cracking that was evident in the products obtained from AMT was far more extensive than that observed for the APT and seemed to have led to a large amount of mechanical breakdown. Consequently, there may be some advantage to be gained by the use of AMT in processes in which rapid rates of reduction and/or small particle sizes are required.

5. Conclusions

(1) Both APT and AMT decompose thermally in a number of well-defined stages.

(2) The decomposition mechanism for APT $(NH_4)_2O:WO_3$ of 5:12, involves the production of AMT, $(NH_4)_2O:WO_3$ of 1:4.

(3) The decomposition of the thermally-produced AMT is the same as the decomposition of chemically-precipitated AMT after its initial dehydration.

(4) The final stages of decomposition of APT and AMT appear to involve the formation of a previously unidentified anhydrous tungstate having a stoichiometry 1:12 $(NH_4)_2O:WO_3$, i.e. of formula $(NH_4)_2O \cdot 12WO_3$.

(5) The final exothermic decomposition stage which occurs for both APT and AMT is explained by the formation of a crystalline solid from an amorphous solid.

References

1. A. K. BASU and F. R. SALE, *J. Mater. Sci.* **10** (1975) 571.
2. T. WILKEN, C. WERT, J. WOODHOUSE and W. MORCOM, *Met. Trans.* 7B (1976) 589.
3. A. K. BASU and F. R. SALE, *Trans. Inst. Min. Metall. (Sect. C: Mineral Process. Ext. Metall.)* 86 (1977) C134.
4. P. TASKINEN and M. H. TIKKANEN, *Scand. J. Met.* 6 (1977) 223.
5. A. K. BASU and F. R. SALE, in Modern Developments in Powder Metallurgy", Vol. 9, edited by H. H. Hausner and P. V. Taubenblatt (Metal Powder Industries Federation and American Powder Metallurgy Institute, New Jersey, 1977) p. 171.
6. A. K. BASU and F. R. SALE, *J. Mater. Sci.* **12** (1977) 1115.
7. V. CHIDA, J. LAFERTY and C. VANDERPOOL, US Patent No. 3,175,881 30. 317,588,130, March 1965.
8. K. LI and C. WANG, "Tungsten – Its History, Geology, Ore Dressing, Metallurgy, Chemistry, Analysis, Application and Economics", (Reinhold, New York, 1955).
9. G. D. RIECK, "Tungsten and its Compounds", (Pergamon Press, New York, 1967).
10. P. G. DICKENS, A. C. HALLIWELL, D. J. MURPHY and M. S. WHITTINGHAM, *Trans. Faraday Soc.* 67 (1971) 794.
11. M. DAHL, Proceedings of the European Symposium on Powder Metallurgy, Stokholm, 1978, Vol. 1, p. 143.
12. L. G. BERG, "Differential Thermal Analysis", (Academic Press, London 1970) p. 350.

Received 28 April and accepted 29 May 1981.